Molecular Dynamics Study of MscL Interactions with a Curved Lipid Bilayer

Grischa R. Meyer,*† Justin Gullingsrud,† Klaus Schulten,† and Boris Martinac*
*School of Medicine and Pharmacology, QEII Medical Centre, University of Western Australia, Crawley WA 6009, Australia; and
†Beckman Institute for Advanced Science and Technology, University of Illinois at Urbana-Champaign, Urbana, Illinois

ABSTRACT Mechanosensitivity is a ubiquitous sensory mechanism found in living organisms. The simplest known mechanotransducing mechanism is found in bacteria in the form of the mechanosensitive membrane channel of large conductance, MscL. This channel has been studied extensively using a variety of methods at a functional and structural level. The channel is gated by membrane tension in the lipid bilayer alone. It serves as a safety valve protecting bacterial cells against hypoosmotic shock. MscL of *Escherichia coli* embedded in bilayers composed of asymmetric amounts of single-tailed and double-tailed lipids has been shown to gate spontaneously, even in the absence of membrane tension. To gain insight into the effect of the lipid membrane composition and geometry on MscL structure, a fully solvated, all-atom model of MscL in a stress-free curved bilayer composed of double- and single-tailed lipids was studied using a 9.5-ns molecular dynamics simulation. The bilayer was modeled as a domed structure accommodating the asymmetric composition of the monolayers. During the course of the simulation a spontaneous restructuring of the periplasmic loops occurred, leading to interactions between one of the loops and phospholipid headgroups. Previous experimental studies of the role of the loops agree with the observation that opening starts with a restructuring of the periplasmic loop, suggesting an effect of the curved bilayer. Because of limited resources, only one simulation of the large system was performed. However, the results obtained suggest that through the geometry and composition of the bilayer the protein structure can be affected even on short timescales.

INTRODUCTION

Mechanosensitive (MS) channels are ubiquitous in most known forms of life (1). They function in mechanotransduction for a wide variety of physiological responses, including hearing and touch reception in mammals and turgor control in bacteria. One of the simplest MS channels discovered is MscL, which exists in the bacterial cytoplasmic membrane and transduces pressure by interaction with the lipid bilayer alone. It protects the bacterium from hypoosmotic shock by allowing the efflux of solutes when the cell membrane is stretched (2). The MscL homolog from *Escherichia coli* has been studied extensively using the patch-clamp technique (3,4) and mutational studies (5–8). With the publication of the three-dimensional crystal structure of the MscL from *Mycobacterium tuberculosis* (9), detailed structural studies and modeling could be carried out (10–16).

Asymmetric addition of amphipaths, including lysophospholipids, lipids with a single fatty acid, to a homogeneous lipid bilayer opens bacterial MS channels even under zero applied pressure (17). Recent electron paramagnetic resonance (EPR) and fluorescent resonance energy transfer (FRET) experiments investigated this effect on MscL in more detail (14,18). It was shown that asymmetric addition of amphipaths to the bilayer increased the opening probability of MscL, leading eventually to full channel opening. It was also shown that short lipids, although they did not open the channel fully, reduced the applied tension required to gate the channel (14).

The asymmetric addition of amphipaths has been shown to induce local curvature into the erythrocyte membrane (19). A change in bilayer shape induced by addition of amphipaths causing membrane curvature is thought to induce the opening of the MS channels (17,20).

Radial forces previously used to accelerate opening of MscL (10,12,16,21) bias all movement in unfortunate ways. The large strength of forces applied accelerates radial movements to a degree that may not allow enough time for movements in other directions to take place before the channel reaches an open state. Furthermore, radial forces could guide the structure along a different opening pathway than that chosen under native conditions. Even though rather convincing suggestions have been advanced by Gullingsrud and Schulten (10), it is not exactly known in what way the protein–lipid interactions exert force on the protein, and the forces assumed in past simulations may have resulted in a nonnative final structure.

Accordingly, we employ in this study a molecular dynamics simulation that does not apply external forces. Instead, we modeled a bilayer of curved shape, incorporating nonbilayer-forming lipids, to directly affect the embedded MscL through the bilayer curvature.

Submitted January 2, 2006, and accepted for publication May 10, 2006.

Address reprint requests to Grischa Meyer at his present address, School of Biomedical Sciences, University of Queensland, Brisbane, QLD 4072, Australia. Tel: 617-3346-1224; Fax: 617-3365-1766; E-mail: grischa@uq.edu.au.

Justin Gullingsrud's present address is University of California, Dept. of Chemistry and Biochemistry, 9500 Gilman Drive, MC-0365, La Jolla, San Diego, CA 92093.

Boris Martinac's present address is School of Biomedical Sciences, University of Queensland, Brisbane QLD 4072, Australia.

0006-3495/06/09/1630/08 $2.00

doi: 10.1529/biophysj.106.080721

Because of the size of the system and limited resources, only one simulation of one bilayer composition was performed. Lacking controls, this ''virtual experiment'' is presented primarily as the first simulation of a curved lipid bilayer, suggesting a geometry and setup that can be used for more exhaustive investigations in the future. The results show details of the MscL gating mechanism that have not been investigated thoroughly before. Although they cannot be regarded as true results, they provide incentive for further experiments.

METHODS

For our investigations, we employed the method of molecular dynamics (MD) simulation (22). The starting point is a computer model of the atomic structure of the protein and its chosen environment, water and lipids in this case. The protein structure of MscL of *E. coli* was taken from the modeling studies by Sukharev et al. (23,24). The cytoplasmic C-terminal region was cut off after residue Ala-110 to reduce system size; it had been shown that this has little effect on the MscL channel activity (8,25).

For the lipid we chose 1,2-dilauroyl-phosphatidylethanolamine (DLPE). This lipid has two fatty acid tails that were chosen much shorter, each only 12 Cs long, than found in common bilayers; however, the chosen lipid furnishes a feasible lipid environment that reduces the opening threshold of MscL as demonstrated in observations (14). To stabilize a nonplanar membrane, we introduced into the two monolayers a heterogeneous distribution (see below) of a single-tail lipid 1-lauroyl-deoxylysophosphatidylcholine (LLPC). The length of LLPC was chosen commensurate with DLPE as 12 Cs.

The scripting abilities of the software package VMD (26) were used to construct first a pure curved (dome-shaped) bilayer as shown schematically in Fig. 1 *A*. For this purpose we employed two sets of mathematical functions for two separate segments describing the lipid dome, segment I (convex) and segment II (concave), as defined in Fig. 1 *A*. The parametric equations describing the bilayer geometry are, for the top layer of segment I,

$$x = (r + t)\sin(\vartheta),\ z = (r + t)\cos(\vartheta) \text{ for } \vartheta \in [0, \varphi]$$

and for the bottom layer of segment I,

$$x = r\sin(\vartheta),\ z = r\cos(\vartheta) \text{ for } \vartheta \in [0, \varphi]$$

for the top layer of segment II

$$x = (2r + t)\sin(\varphi) - r\sin(\vartheta),$$
$$z = (2r + t)\cos(\varphi) - r\cos(\vartheta) \text{ for } \vartheta \in [0, \varphi]$$

and for the bottom layer of segment II

$$x = (2r + t)\sin(\varphi) - (r + t)\sin(\vartheta),$$
$$z = (2r + t)\cos(\varphi) - (r + t)\cos(\vartheta) \text{ for } \vartheta \in [0, \varphi]$$

where r is the radius of curvature, t the thickness of the bilayer, and φ the angle of the circle segment. The curved bilayer for this study has $r = 68$ Å (1 Å $= 10^{-10}$ m), $t = 36$ Å, and $\varphi = 44°$. The bilayer results from a rotation of both segments around the z axis (*dashed line* in Fig. 1 *A*).

The dome shape of the curved bilayer was realized through a particular distribution of the DLPE and LLPC lipids. In the convex segment, I, LLPC was placed in the outer monolayer; in the concave segment, II, the LLPC lipids were placed in the inner monolayer. Altogether we placed 424 DLPE and 105 LLPC lipids in the top monolayer and 288 DLPE and 217 LLPC lipids in the bottom monolayer. A 1:1 ratio of LLPC and DLPE lipids was chosen, which is larger than the 1:3 ratio employed in the EPR experiments (14). The reason for this choice is to cause a pronounced effect of the bilayer on the inserted MscL to elicit an effect on the protein on the short (10-ns) time scale of the simulations (see below).

The protein was placed into the center of the bilayer using VMD (26), deleting all overlapping lipids. The method has been described numerous times, e.g., in Gullingsrud et al. (16). The protein lipid bilayer system was then solvated in a bath of explicit water molecules, again following earlier procedures (10). The boundary of the overall system was chosen to be a hexagonal prism with a side length of 109 Å and a height of 114 Å. The entire system consisted of 276,167 atoms, 8745 protein atoms in five monomers of 110 residues each, the remaining atoms stemming from 1034 lipids and 58,588 water molecules. Fig. 1 *C* shows an overall view of the system, and Fig. 1 *B* presents a cut through the system after 2 ns of equilibration.

Molecular dynamics simulations were performed using the program NAMD2 (27) together with the CHARMM27 force field for lipids (28,29)

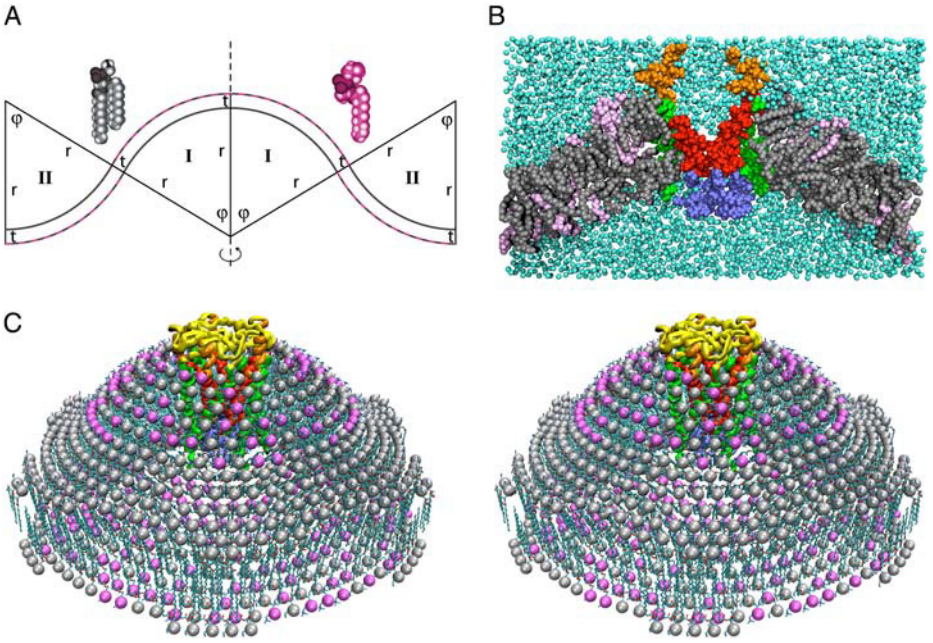

FIGURE 1 (*A*) Two-dimensional representation of the curved bilayer. The curvature is induced by a heterogeneous distribution of single-tailed lipids (*pink*), that form the upper (lower) monolayer in regions I (II), and doubletailed lipids (*gray*), that form the lower (upper) monolayer in regions I (II). The quantities shown, r, t, φ, are used to describe mathematically the curved bilayer (see Methods). (*B*) A slice through the center of the protein-lipid-water system after 2 ns of simulation. Lipids and the MscL protein are color-coded as in *C*, except that the periplasmic loops are shown in orange. Water molecules are presented in turquoise. (*C*) Stereo view of the lipid bilayer and the MscL protein before equilibration. Water molecules are not shown. Single-tailed lipids are presented in pink, double-tailed lipids in gray. MscL is colored as in Fig. 3.

and CHARMM22 for proteins (30,31). For all but the first 470 ps of the simulation, the bonds to all hydrogen atoms were kept rigid using the SHAKE algorithm (32). This permitted a time step of 2 fs to be used. The simulation was performed with periodic boundary conditions accounting for full electrostatics described by means of the particle mesh Ewald (PME) method (33) with a grid spacing of 1 Å or less. The temperature was kept at 300 K using Langevin dynamics on all but the hydrogen atoms with a damping coefficient of 5 ps^{-1}. During the simulations the pressure was kept constant at 1.013 bar, but the size of the simulation cell was allowed to change.

Simulations started with a 3000-step minimization of the entire protein-lipid water system that removed all unfavorable steric contacts. The system was then heated for 6 ps at a time step of 1 fs up to 300 K using Langevin dynamics (34). The C_α-atoms of the protein were constrained to their initial position during heating. The system was equilibrated first for 228 ps with a time step of 1 fs and C_α-atoms constrained. The next 231 ps were performed without the constraints. For the remainder of the simulation, the SHAKE (32) algorithm was used to constrain the bonds to hydrogen atoms, as pointed out above. After the equilibration phase, the system was permitted free dynamics for an extensive period of 9.5 ns and monitored for analysis using VMD (26). The simulations were carried out on a 750 AlphaServer ES45 node computer cluster at the Pittsburgh Supercomputer Center. On 512 processors 1-ns dynamics required 9 h.

RESULTS

The root mean-squared deviation (RMSD) from the initial MscL structure is shown in Fig. 2. The periplasmic loops (residues I-40 to Y-75) moved the most, whereas the gating region (residues 20–28) moved the least. The pore of the open channel has a minimum diameter of 25 Å (13), but the pore diameter of the closed channel did not change significantly during the 9.5-ns simulation. Calculations using HOLE (35) showed that the minimum pore did not change significantly in magnitude and position, remaining at ~1.4 Å. Hence, the channel did not reach an open or subconducting state during the simulation time.

Fig. 3 shows the side and top views of the protein at the beginning and end of the simulation. The large movements of the periplasmic loop are the most visible changes in the protein's structure.

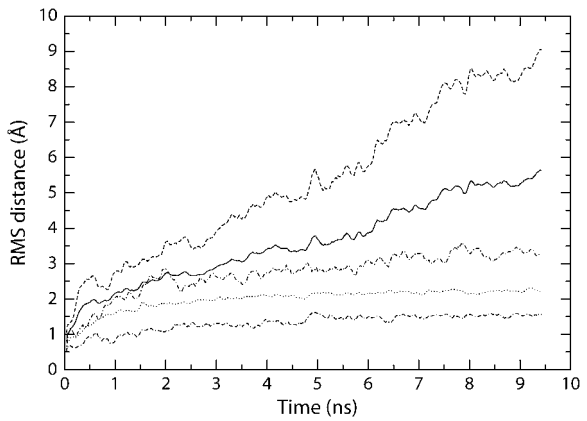

FIGURE 2 Time development of the RMSD of MscL. The RMSD values shown were determined for the C_α-atoms only and correspond to the whole protein (*solid line*), the periplasmic loops (*dashed line*), the transmembrane helices (*dotted line*), the gating region, i.e., residues A-20 to A-28 (*dash-dash-dotted line*), and the N-terminal (S1) helices (*dash-dotted line*).

For comparison with recent EPR experiments (13,14), the rotation of helices was measured using a vector between the center of mass of the backbone of the helix and the two helices of opposing subunits. The helix in question was fixed, and the movement of the other two helices was measured. Fig. 4 *A* indicates a 20° rotation after 7 ns of the hydrophobic gate part formed by the TM1 helix. This is accompanied by an inverse rotation of the upper part (residues I-32 to I-40, not shown) of the same helix.

This behavior is not repeated in the other subunits. Subunits 2 and 5 exhibit a rotation of 20° and 15°, respectively, of the lower part of TM1. The upper part of TM1 in subunit 2 rotates in the same way as the lower part.

The rotational movements of subunit 1 are related to the breakdown of the α-helix backbone hydrogen bonding between residues A-28 and I-32. Fig. 4 *B* shows that at first the TM1 helix kinks at this position and in the end straightens again. A plot of the distance between the hydrogen-bonding atoms of I-28 and I-32, shown in Fig. 4 *C*, reveals a possible correlation with the rotational movements outlined above. When the different parts of TM1 rotate after 7 ns, the hydrogen bond reforms. The TM2 helix of subunit 1 goes through a bending motion simultaneously.

The helix structures of the other subunits stay intact throughout the whole simulation. However, subunit 3 exhibits TM1 helix bending, which resembles the bending and breakdown of structure seen in subunit 1 (data not shown), suggesting a common mechanism.

In the initially modeled structure, residues M-42 to Y-75 form a ring with 4.9-Å radius around the top. During the simulation all of the five subunits' loops changed significantly from their initial conformations. As can be seen from an RMSD analysis (Fig. 2), none of the loops have reached a stable conformation by the end of the simulation. One of the loops exhibits an interesting behavior involving interaction with the lipid headgroups after ~9 ns.

Fig. 5 *A* shows the hydrogen-bonding interactions of periplasmic residues with lipid headgroups. In the equilibrated protein in its closed form, residues 39 to 43 and 78, 79, 82, and 83, but not the loop in between, are interacting with the lipid headgroups. Glutamine residue Q-65 of subunit 1 is a notable exception to that set of interacting residues, as it is located at the tip of the loop, which sits on top of the channel. Due to the interactions the lipid molecules involved rose slightly above the level of the neighboring lipids.

Three of the other subunits, subunits 2, 3, and 4, unfold in a similar manner to subunit 1, but not as fast, and move more upward than outward. No unusual lipid interactions developed during the 9.5 ns. Subunit 5 unfolds inward, occluding the pore further. This is why the pore diameter at the periplasmic loop stays nearly constant from the beginning to the end (data not shown).

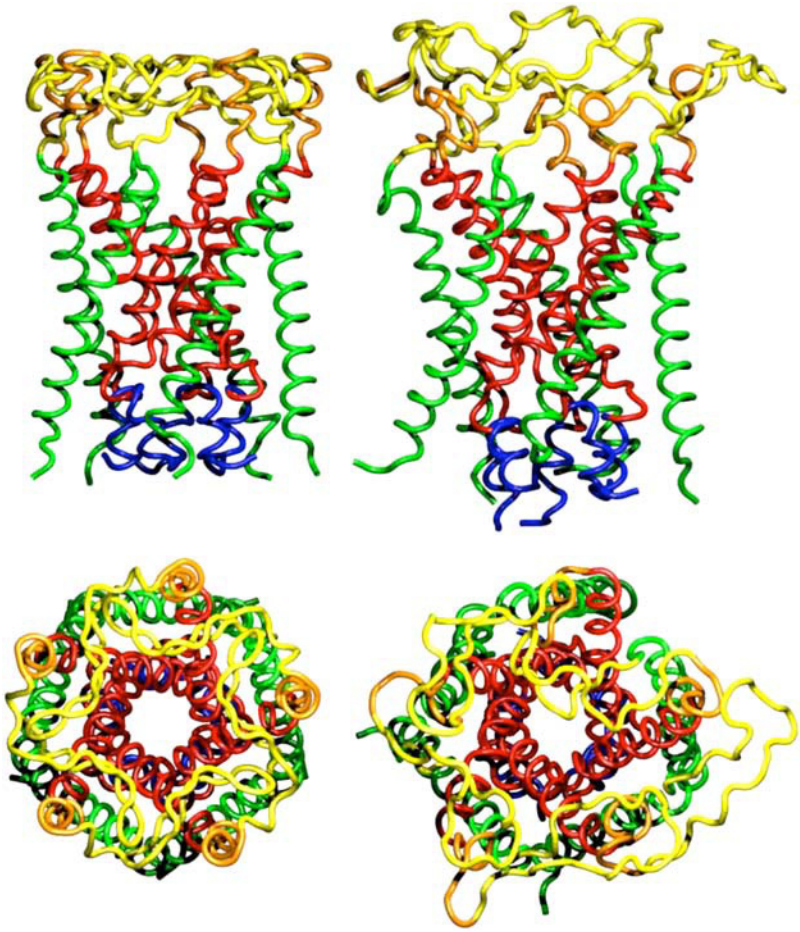

FIGURE 3 MscL at the beginning (*left*) and end (*right*) of the 9.5-ns simulation. Shown are the N-terminal helices S1 (*blue*), the transmembrane helices TM1 (*red*), the periplasmic helices S2 (*orange*), the periplasmic loops S2 (*yellow*), and the transmembrane helices TM2 (*green*). The C-terminus (S3) has been cut off in our simulation and is not shown.

The bilayer thickness was measured between the phosphorus atoms of the lipid headgroups, as shown in Fig. 5 *B*. The native thickness of the bilayer used in the simulation is much thinner, <30 Å. The lipids near the protein first come together, closer to the native thickness, as they had not yet interacted with the protein much (see Fig. 4 *A*). As these interactions increase, from 3.2 ns onward, the bilayer thickness near the protein expands to almost 35 Å thickness, matching the protein's hydrophobic region, whereas the overall bilayer retains its initial low thickness of slightly <30 Å. The increase in protein–lipid contacts after 3.2 ns is also visible in Fig. 5 *A*.

The bilayer remains stable throughout the whole simulation time. However, the bilayer does not keep its initial ideal dome shape. The amount of curvature is slightly reduced, and the beginning of slow undulations is apparent around the perimeter of the dome.

The total surface tension is small, and the system stays stress-free during all but the initial few steps of the simulation, as shown by the near constant area and height of the simulation box (Fig. 1, supplementary material). Previous simulations suggest that a rapid change in area would be seen if the tension were far from zero (36).

To confirm that the biologically relevant liquid crystal phase prevails in our DLPE/LLPC bilayer, we calculated the lipid order parameter for DLPE and LLPC separately, at several time points in the simulation, using the standard expression $S_{CD} = \langle 3/2 \cos^2\theta - 1/2 \rangle$, where θ is the angle between each C-H bond and the bilayer normal. This parameter is directly comparable to the deuterium order parameter, which is experimentally measurable through quadrupole splittings (37). The curvature of the bilayer was taken into account at each lipid position by defining the local bilayer normal as a vector from a given lipid to its nearest neighbor in the opposite leaflet. We tested this algorithm on flat bilayers and found that it produced results within 5% of what one would obtain using an idealized normal aligned with a Cartesian axis.

The order parameters for the DLPE acyl chains were found to stabilize within 2 ns, whereas the corresponding values for the single LLPC chain increased by ~15% during the entire simulation. Average order parameters averaged over the final 5 ns are shown in Fig. 5 *C*. The DLPE parameters compare very well to previous simulations of flat DLPE bilayers in the liquid crystalline state (38, Fig. 3). Compared to experimental values for DLPC (39), our order parameters for DLPE are slightly higher, as might be expected from the smaller headgroup of DLPE (38). The LLPC chains are seen to be slightly more ordered than those of DLPE, possibly

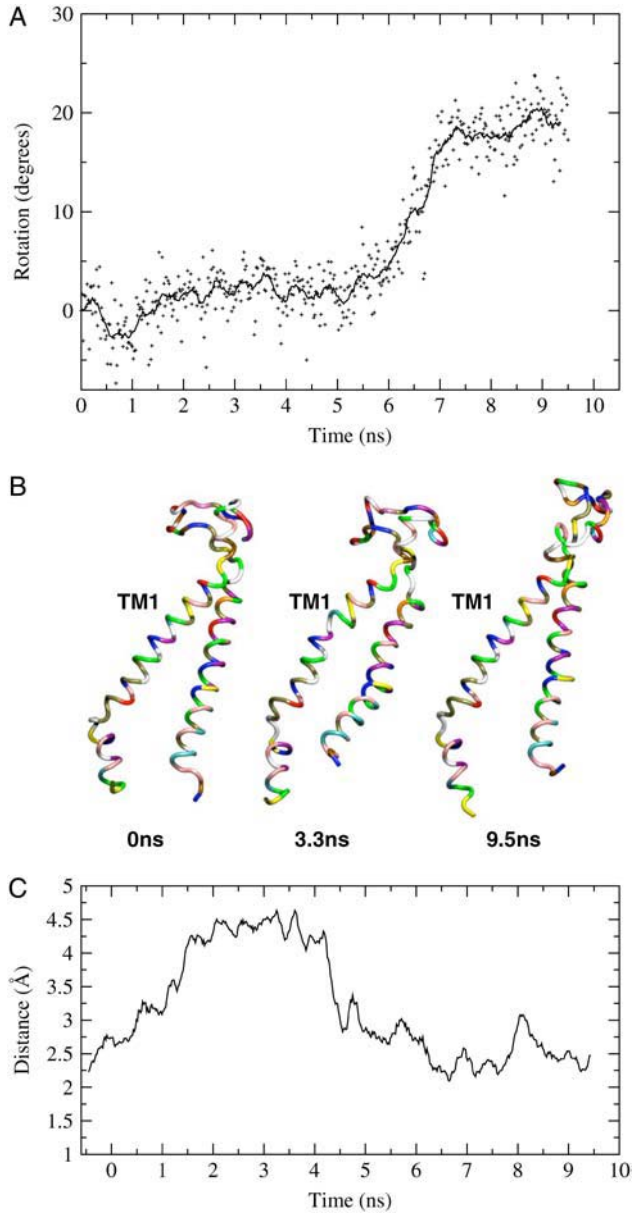

FIGURE 4 (*A*) Rotation of the gating region of subunit 1 (residues A-20 to A-28). The gating region is seen to rotate during the simulation relative to the remaining MscL. The dots represent snapshots from the simulation; the line represents a running average (over a 100-ps window). (*B*) Conformational dynamics of subunit 1. Shown are conformations of the subunit (helices TM1 and TM2) at the beginning of the simulation, at 3.3 ns, and at the end of the simulation. (*C*) Time development of the distance between hydrogen-bonding atoms of A-28 and I-32.

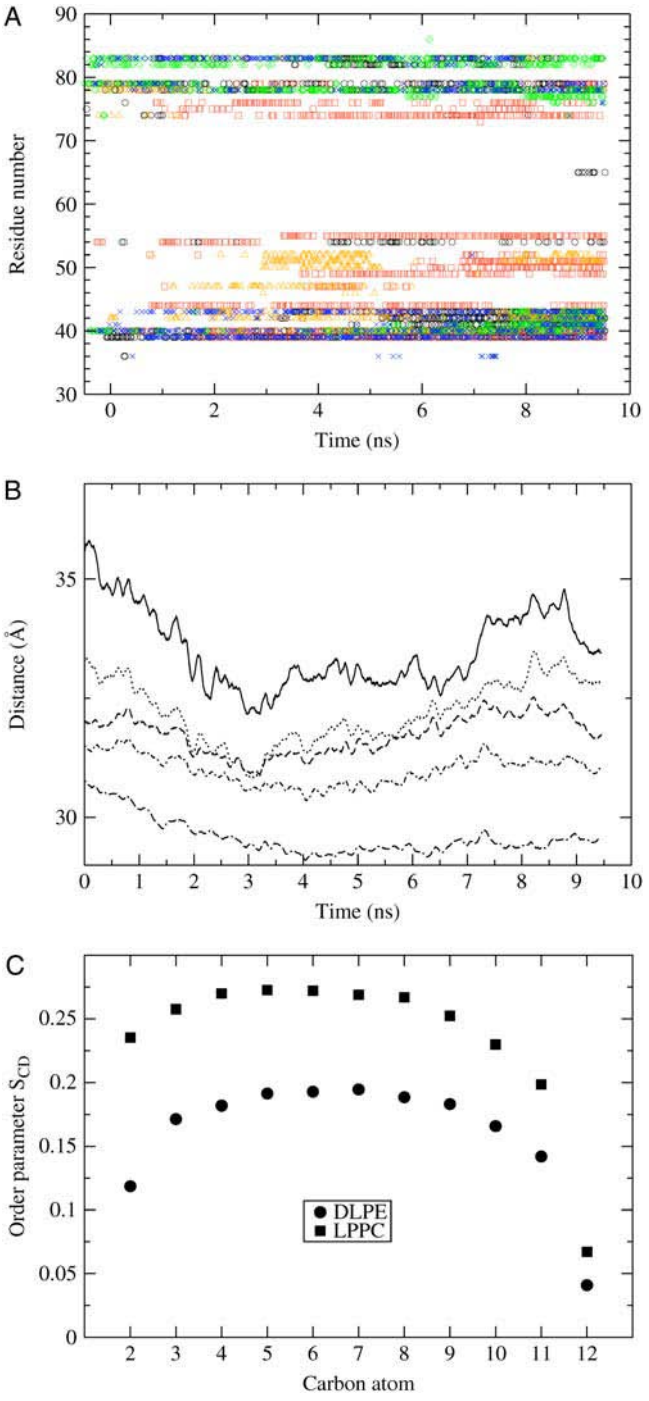

FIGURE 5 (*A*) Time development of lipid-protein interaction. For each event in which lipid headgroups and protein side groups approach each other to <3 Å, a symbol is shown for the respective side group. Colors differentiate side groups of subunit 1 (*black circle*), 2 (*red square*), 3 (*green diamond*), 4 (*blue cross*), and 5 (*orange triangle*). (*B*) Thickness of the lipid bilayer. The thickness is measured as the distance between the phosphorus atoms. Shown are averages encompassing the phosphorus atoms at radii 10 Å (*solid*), 20 Å (*dotted*), 30 Å (*dashed*), and 40 Å (*dash-dotted*) from the protein, and all phosphorus atoms (*dash-dash-dotted*). (*C*) Deuterium order parameter $S_{CD} = \langle 3/2 \cos^2 \theta - 1/2 \rangle$, where θ is the angle between each C-H bond and the bilayer normal. Shown are the order parameters at each acyl chain carbon for the DLPE (double-tailed) and LLPC (single-tailed) lipids.

reflecting the increased area available to the DLPE chains imparted by the glycerol chain.

DISCUSSION

The molecular dynamics (MD) simulation presented here used a new strategy to affect the MscL structure differing in this regard from previous studies (10–12,16,21,38).

Although the application of external forces in previous simulations allowed a greater range of the gating process to be investigated, the results from such simulations may have a bias that is difficult to discern. Experimentally, intrinsic forces between an asymmetric bilayer and the protein induce an opening of the MscL channel (14,18). The curved membrane employed in the current study, although nearly stress-free, may be closer to the actual experimental geometry than a perfectly planar bilayer and in any case afforded us the opportunity to study the stability of simulated lipid bilayers in this novel arrangement and its possible effects on gating of the embedded MscL. Because of the limitations of current computer power, only the very early (9.5 ns) stages of gating could be covered in our 276,000-atom simulation, the large simulation volume being necessary to accommodate the domed bilayer. Control and repeat simulations were also beyond the resources available. However, to properly evaluate the role played by the bilayer shape and composition and estimate its stability over time, control simulations and longer simulations would need to be performed. Hence, the presented interpretations are to be seen not as facts but as suggestions for further studies of bilayers, proteins, and curvature using the novel method of a dome-shaped bilayer.

The RMSD values show that the only parts of the structure that undergo major rearrangements in our simulations are the periplasmic loops and extracellular helices. There are two possible reasons for these rearrangements. One is that the model may be incorrect in that region. Uncertainties in the model have been acknowledged by Sukharev et al. (24). The other reason, which is founded on experimental observations, may be that the curved bilayer environment guides the channel toward the open state. Naturally, we permit ourselves to believe that the second possibility is actually reflecting a native response of MscL. We learn then from our simulations that the rearrangement of some of the MscL loops could play an important role in MscL's gating mechanism. As explained in the Introduction, previous simulations could not resolve this step because they emphasized, through the application of strong radial forces, large-scale rearrangements of the TM helices (10,12,16,21) or targeted an assumed final structure for the protein (15).

The periplasmic loop of MscL has been shown to play a significant role in the channel gating. Ajouz et al. (40) demonstrated that cutting of the loops by proteases increased dramatically MscL pressure sensitivity, which led to a proposal that the periplasmic loop functions as a spring resisting the movement of the transmembrane helices that underlie the critical event in mechanical gating of MscL. This proposal received support from a recent study showing that coreconstitution of the N- and C-terminal halves of MscL into liposomes yielded mechanosensitive channels exhibiting increased sensitivity to bilayer tension (41). Together, both studies seem to support our assumption that the unfolding of the loop may present the initial step in the opening of MscL. A cut in the loop makes it easier for both ends to move freely and to unfold or refold. If it were necessary for the channel opening that the loops unfold, the cut would make this step easier. Experimental studies of the periplasmic loop residue Q-65 have further confirmed the important role of the periplasmic loop in the gating process (42).

A less visible feature, the rotation of some of the TM helices, could possibly be related to previous experimental findings in which closed intermediate states of MscL (13) showed similar movements. Models based on EPR measurements of a closed intermediate conformation predict 30° rotation (per subunit on average) from the closed initial state to a (yet) closed intermediate state (13). In the simulation, we see a 20° rotation for one subunit, less for the others.

At least in one subunit, the rotation is linked to a breakdown of secondary structure in the TM1 helix and bending in TM2. Bending or kinking of the TM helices has been suggested to be important in the mechanism of ion-channel gating as well as for the functional control of other proteins (43,44) and has been observed in an MD simulation (15) as well as by normal-mode analysis (45). The kink in the first TM helix occurs in a region of well-conserved residues of the gating region. In a new MD simulation of the mechanosensitive channel of small conductance, MscS, embedded in a lipid bilayer (46), similar kinks in the homologous region of conserved residues in the inner TM helix were observed. The agreement with experimental results for the MscL gating mechanisms supports our assumption that the curved bilayer affects the structure of the embedded MscL and leads it toward opening.

The interaction between the protein and lipids is also in agreement with experiments. Hydrophobic matching was to be expected and agrees with what has been postulated for membrane proteins previously (2,47–52). Fig. 5 *B* clearly shows that matching of the bilayer thickness to the protein's hydrophobic region occurred over time. The correlation with the increase of lipid-protein interactions is visible in Fig. 5 *A*.

Although we did not apply global tension, and the system is overall stress-free, we are aware that this might not be true locally. The local pressure profiles of the curved bilayer would deserve further investigation similar to what has been done for planar bilayers (38). We were already at the limit of available computer power for this 280,000-atom, 10-ns simulation, and the bilayer is still undergoing adjustments to its curvature. An even longer simulation would be necessary to gather good statistics on the lateral pressure, especially if it is desired to find the local pressure near the protein. Fortunately, NAMD has been updated recently to permit pressure profile analysis with partitions by atom type (53); this new feature will serve future analysis of curved membrane simulations.

CONCLUSION

The results of the single molecular dynamics simulation that is presented in this study cannot change our current

schematic view of MscL gating, an irislike expansion of the TM helices. They suggest, however, that some of the detailed conformational transitions involved in the gating mechanism, including kinked TM helices as well as the role of the periplasmic loops, have yet to be determined experimentally to arrive at a complete model of MscL gating. For this purpose, experimental investigations of the extracellular domain are needed: its part in the opening mechanism begs to be determined. Furthermore, the work presented here also demonstrates that curved bilayers are stable in simulation and lays the groundwork for more in-depth stressed and curved bilayer simulations. The results suggest that the desired effect of the bilayer on protein structure was achieved. To take the curved bilayer method further, different MD simulations need to be undertaken. A statistically representative number of simulations of the bilayer without protein, of a planar heterogenic bilayer, and of a curved homogenic bilayer, all over longer times, are necessary.

SUPPLEMENTARY MATERIAL

An online supplement to this article can be found by visiting BJ Online at http://www.biophysj.org.

We thank members of the Theoretical and Computational Biophysics Group for helpful discussions.

This work was supported by the National Institutes of Health (NIH P41 RR05969 and NIH 1 RO1 GM067887-01) and by the Australian Research Council (ARC DP0342581). The authors also acknowledge computer time provided by the National Science Foundation NRAC Grant MCA93S028. Some of this work was conducted while Grischa Meyer was International Postgraduate Research Scholar in Australia. The molecular images in this article were created with the molecular graphics program VMD (26).

REFERENCES

1. Martinac, B. 2004. Mechanosensitive ion channels: molecules of mechanotransduction. *J. Cell Sci.* 117:2449–2460.
2. Hamill, O., and B. Martinac. 2001. Molecular basis of mechanotransduction in living cells. *Physiol. Rev.* 81:685–740.
3. Sukharev, S., W. Sigurdson, C. Kung, and F. Sachs. 1999. Energetic and spatial parameters for gating of the bacterial large conductance mechanosensitive channel, MscL. *J. Gen. Physiol.* 113:525–540.
4. Häse, C., A. Le Dain, and B. Martinac. 1995. Purification and functional reconstitution of the recombinant large mechanosensitive ion channel (MscL) of *Escherichia coli*. *J. Biol. Chem.* 270:18329–18334.
5. Maurer, J., and D. Dougherty. 2003. Generation and evaluation of a large mutational library from the *Escherichia coli* mechanosensitive channel of large conductance, MscL: implications for channel gating and evolutionary design. *J. Biol. Chem.* 278:21076–21082.
6. Yoshimura, K., A. Batiza, and C. Kung. 2001. Chemically charging the pore constriction opens the mechanosensitive channel MscL. *Biophys. J.* 80:2198–2206.
7. Ou, X., P. Blount, R. Hoffman, and C. Kung. 1998. One face of a transmembrane helix is crucial in mechanosensitive channel gating. *Proc. Natl. Acad. Sci. USA.* 95:11471–11475.
8. Blount, P., S. I. Sukharev, M. J. Schroeder, S. K. Nagle, and C. Kung. 1996. Single residue substitutions that change the gating properties of a mechanosensitive channel in *Escherichia coli*. *Proc. Natl. Acad. Sci. USA.* 93:11652–11657.
9. Chang, G., R. Spencer, A. Lee, M. Barclay, and D. Rees. 1998. Structure of the MscL homolog from *Mycobacterium tuberculosis:* a gated mechanosensitive ion channel. *Science.* 282:2220–2226.
10. Gullingsrud, J., and K. Schulten. 2003. Gating of MscL studied by steered molecular dynamics. *Biophys. J.* 85:2087–2099.
11. Elmore, D., and D. Dougherty. 2003. Investigating lipid composition effects on the mechanosensitive channel of large conductance (MscL) using molecular dynamics simulations. *Biophys. J.* 85:1512–1524.
12. Colombo, G., S. Marrink, and A. Mark. 2003. Simulation of MscL gating in a bilayer under stress. *Biophys. J.* 84:2331–2337.
13. Perozo, E., D. Cortes, P. Sompornpisut, A. Kloda, and B. Martinac. 2002. Open channel structure of MscL and the gating mechanism of mechanosensitive channels. *Nature.* 418:942–948.
14. Perozo, E., A. Kloda, D. Cortes, and B. Martinac. 2002. Physical principles underlying the transduction of bilayer deformation forces during mechanosensitive channel gating. *Nat. Struct. Biol.* 9:696–703.
15. Kong, Y., Y. Shen, T. Warth, and J. Ma. 2002. Conformational pathways in the gating of *Escherichia coli* mechanosensitive channel. *Proc. Natl. Acad. Sci. USA.* 99:5999–6004.
16. Gullingsrud, J., D. Kosztin, and K. Schulten. 2001. Structural determinants of MscL gating studied by molecular dynamics simulations. *Biophys. J.* 80:2074–2081.
17. Martinac, B., J. Adler, and C. Kung. 1990. Mechanosensitive ion channels of *E. coli* activated by amphipaths. *Nature.* 348:261–263.
18. Corry, B., P. Rigby, Z. W. Liu, and B. Martinac. 2005. Conformational Changes involved in MscL channel gating measured using FRET spectroscopy. *Biophys. J.* 89:L49–L51.
19. Sheetz, M., and S. Singer. 1974. Biological membranes as bilayer couples. A molecular mechanism of drug–erythrocyte interactions. *Proc. Natl. Acad. Sci. USA.* 71:4457–4461.
20. Patel, A., E. Honore, F. Maingret, F. Lesage, M. Fink, F. Duprat, and M. Lazdunski. 1998. A mammalian two pore domain mechano-gated S-like K^+ channel. *EMBO J.* 17:4283–4290.
21. Bilston, L., and K. Mylvaganam. 2002. Molecular simulations of the large conductance mechanosensitive (MscL) channel under mechanical loading. *FEBS Lett.* 512:185–190.
22. Frenkel, D., and B. Smit. 1996. Understanding Molecular Simulation: From Algorithms to Applications. Academic Press, San Diego, CA.
23. Sukharev, S., M. Betanzos, C. Chiang, and H. Guy. 2001. The gating mechanism of the large mechanosensitive channel MscL. *Nature.* 409:720–724.
24. Sukharev, S., S. Durell, and H. Guy. 2001. Structural models of the MscL gating mechanism. *Biophys. J.* 81:917–936.
25. Häse, C., A. Le Dain, and B. Martinac. 1997. Molecular dissection of the large mechanosensitive ion channel (MscL) of *E. coli:* mutants with altered channel gating and pressure sensitivity. *J. Membr. Biol.* 157:17–25.
26. Humphrey, W., A. Dalke, and K. Schulten. 1996. VMD–visual molecular dynamics. *J. Mol. Graph.* 14:33–38.
27. Phillips, J. C., R. Braun, W. Wang, J. Gumbart, E. Tajkhorshid, E. Villa, C. Chipot, R. D. Skeel, L. Kale, and K. Schulten. 2005. Scalable molecular dynamics with NAMD. *J. Comput. Chem.* 26:1781–1802.
28. Feller, S., D. Yin, R. Pastor, and A. MacKerell Jr. 1997. Molecular dynamics simulation of unsaturated lipid bilayers at low hydration: parameterization and comparison with diffraction studies. *Biophys. J.* 73:2269–2279.
29. Schlenkrich, M., J. Brickmann, A. D. MacKerell Jr., and M. Karplus. 1996. Empirical potential energy function for phospholipids: Criteria for parameter optimization and applications. *In* Biological Membranes: A Molecular Perspective from Computation and Experiment. K. M. Merz and B. Roux, editors. Birkhauser, Boston. 31–81.
30. MacKerell, A. D. Jr., D. Bashford, M. Bellott, R. L. Dunbrack, M. J. Field, S. Fischer, J. Gao, H. Guo, S. Ha, D. Joseph, L. Kuchnir, K.

Kuczera, F. T. K. Lau, C. Mattos, S. Michnick, D. T. Nguyen, T. Ngo, B. Prodhom, B. Roux, M. Schlenkrich, J. Smith, R. Stote, J. Straub, J. Wiorkiewiczkuczera, and M. Karplus. 1992. Self-consistent parameterization of biomolecules for molecular modeling and condensed phase simulations. *FASEB J.* 6:A143.

31. MacKerell, A. D. Jr., D. Bashford, M. Bellott, R. L. Dunbrack, J. D. Evanseck, M. J. Field, S. Fischer, J. Gao, H. Guo, S. Ha, D. Joseph-McCarthy, L. Kuchnir, K. Kuczera, F. T. K. Lau, C. Mattos, S. Michnick, T. Ngo, D. T. Nguyen, B. Prodhom, W. E. Reiher, B. Roux, M. Schlenkrich, J. C. Smith, R. Stote, J. Straub, M. Watanabe, J. Wiorkiewicz-Kuczera, D. Yin, and M. Karplus. 1998. All-atom empirical potential for molecular modeling and dynamics studies of proteins. *J. Phys. Chem. B.* 102:3586–3616.
32. Ryckaert, J., G. Ciccotti, and H. J. C. Berendsen. 1977. Numerical integration of the Cartesian equations of motion of a system with constraints: molecular dynamics of *n*-alkanes. *J. Comput. Phys.* 23: 327–341.
33. Darden, T., D. York, and L. Pedersen. 1993. Particle mesh Ewald—an *N*.Log(*N*) method for Ewald sums in large systems. *J. Chem. Phys.* 98: 10089–10092.
34. Pastor, R. W., B. R. Brooks, and A. Szabo. 1988. An analysis of the accuracy of Langevin and molecular dynamics algorithms. *Mol. Phys.* 65:1409–1419.
35. Smart, O., J. Goodfellow, and B. Wallace. 1993. The pore dimensions of gramicidin A. *Biophys. J.* 65:2455–2460.
36. Feller, S. E., and R. W. Pastor. 1999. Constant surface tension simulations of lipid bilayers: The sensitivity of surface areas and compressibilities. *J. Chem. Phys.* 111:1281–1287.
37. Seelig, J. 1977. Deuterium magnetic resonance: theory and application to lipid membranes. *Q. Rev. Biophys.* 10:353–418.
38. Gullingsrud, J., and K. Schulten. 2004. Lipid bilayer pressure profiles and mechanosensitive channel gating. *Biophys. J.* 86:3496–3509.
39. Petrache, H. I., S. W. Dodd, and M. F. Brown. 2000. Area per Lipid and Acyl Length Distributions in Fluid Phosphatidylcholines Determined by 2H NMR Spectroscopy. *Biophys. J.* 79:3172–3192.
40. Ajouz, B., C. Berrier, M. Besnard, B. Martinac, and A. Ghazi. 2000. Contributions of the different extramembranous domains of the mechanosensitive ion channel MscL to its response to membrane tension. *J. Biol. Chem.* 275:1015–1022.
41. Park, K. H., C. Berrier, B. Martinac, and A. Ghazi. 2004. Purification and Functional Reconstitution of N- and C-halves of the MscL channel. *Biophys. J.* 86:2129–2136.
42. Tsai, I. J., Z. W. Liu, J. Rayment, C. Norman, A. McKinley, and B. Martinac. 2005. The role of the periplasmic loop residue glutamine 65 for MscL mechanosensitivity. *Eur. Biophys. J.* 34:403–412.
43. Sansom, M., and H. Weinstein. 2000. Hinges, swivels and switches: the role of prolines in signalling via transmembrane alpha-helices. *Trends Pharmacol. Sci.* 21:445–451.
44. Doyle, D. A. 2004. Structural changes during ion channel gating. *Trends Neurosci.* 27:298–302.
45. Valadie, H., J. Lacapcre, Y. Sanejouand, and C. Etchebest. 2003. Dynamical properties of the MscL of *Escherichia coli:* a normal mode analysis. *J. Mol. Biol.* 332:657–674.
46. Sotomayor, M., and K. Schulten. 2004. Molecular dynamics study of gating in the mechanosensitive channel of small conductance MscS. *Biophys. J.* 87:3050–3065.
47. Tieleman, D. P., L. R. Forrest, M. S. Sansom, and H. J. Berendsen. 1998. Lipid properties and the orientation of aromatic residues in OmpF, influenza M2, and alamethicin systems: molecular dynamics simulations. *Biochemistry.* 37:17554–17561.
48. Dumas, F., M. C. Lebrun, and J. F. Tocanne. 1999. Is the protein/lipid hydrophobic matching principle relevant to membrane organization and functions? *FEBS Lett.* 458:271–277.
49. Mouritsen, O. G., and M. Bloom. 1984. Mattress model of lipid-protein interactions in membranes. *Biophys. J.* 46:141–153.
50. Mouritsen, O. G., and M. Bloom. 1993. Models of lipid-protein interactions in membranes. *Annu. Rev. Biophys. Biomol. Struct.* 22: 145–171.
51. Mouritsen, O. G., and M. M. Sperotto. 1993. Thermodynamics of lipid-protein interactions in lipid membranes. *In* The Hydrophobic Matching Condition. M. Jackson, editor. CRC Press, Boca Raton, FL.
52. Mouritsen, O. G., B. Dammann, H. C. Fogedby, J. H. Ipsen, C. Jeppesen, K. Jorgensen, J. Risbo, M. C. Sabra, M. M. Sperotto, and M. J. Zuckermann. 1995. The computer as a laboratory for the physical-chemistry of membranes. *Biophys. Chem.* 55:55–68.
53. Gullingsrud, J., A. Babakhani, and J. A. McCammon. 2006. Computational investigation of pressure profiles in lipid bilayers with embedded proteins. *Mol. Simul.* In press.